Journal of MATERIALS RESEARCH

Article
DOI: 10.1557/jmr.2019.309

Multifunctional antifogging coatings based on ZrO_2 and SiO_2 nanoparticles by spray-spin-blow layer-by-layer assembly

Fusheng Yang[1,a),b)], Changlong Li[1,b)], Wenzheng Xu[2], Zaisheng Cai[3]

[1]College of Textiles and Clothing, Anhui Polytechnic University, Wuhu, Anhui 241000, China; and Key Lab of Textile Science & Technology of Anhui Province, Anhui Polytechnic University, Wuhu, Anhui 241000, China
[2]College of Textiles and Clothing, Anhui Polytechnic University, Wuhu, Anhui 241000, China
[3]College of Chemistry, Chemical Engineering and Biotechnology, Donghua University, Shanghai 201620, China
[a)]Address all correspondence to this author. e-mail: eyangfs@sina.com
[b)]These authors contributed equally to this work.

Received: 14 August 2019; accepted: 24 September 2019

Multifunctional antifogging (AF) coatings consisting of alternating layers of positively charged ZrO_2 nanoparticles (NPs) and negatively charged SiO_2 NPs were rapidly fabricated via spray-spin-blow layer-by-layer electrostatic assembly followed by calcination. The resultant coatings of only three bilayers exhibited excellent AF, superhydrophilic, antireflective (AR), and self-cleaning (SC) properties, as well as high mechanical stability. These were demonstrated by various methods, e.g., transmission and scanning electron microscopy, X-ray diffraction, UV-Vis spectrometry, a contact angle test, a boiling test (constant 100 °C), a low-temperature test, and mechanical stability tests. ZrO_2 and SiO_2 NPs were synthesized and utilized as building blocks for fabricating the coatings. The resultant coatings exhibited excellent AF and SC properties due to the superhydrophilicity of the coating, showed excellent AR properties due to the quarter-wave coating with a low refractive index, and exhibited excellent superhydrophilic properties due to a rough microtextured surface. The simplicity of the fabrication process, easy availability of the nanomaterials, and excellent adhesion to substrates for the coating preparation might make the low-cost, nontoxic, and eco-friendly multifunctional coatings potentially useful in optical and display devices.

Introduction

Fogging occurs when the hot water vapor condenses onto a cold surface to form discrete and dispersed light-diffusing tiny droplets and when the surface temperature is below the dew point of the surrounding air [1, 2, 3]. Fogging is quite common and often causes trouble to people in day-to-day life. To solve the problem, we can fabricate a coating, which is wetted by water completely and instantaneously (superhydrophilicity: water contact angle $< 5°$ within 0.5 s or less) [4, 5] or which completely resists wetting by water (superhydrophobicity: water contact angle $> 150°$ and very low sliding angle $< 5°$; $<$ 6-μL droplets) [6, 7]. To obtain a highly transparent surface, we should construct antireflective (AR) coatings. Nowadays, AR coatings/films have been attracting much attention for their applications in solar cells, optical devices, and display devices as a result of their ability to enhance transmittance and remove ghost images [8, 9]. An ideal AR coating should match the following two conditions [10]: (i) $n_c = (n_a \times n_s)^{1/2}$, reflection will be suppressed at the wavelength near the quarter-wavelength optical thickness of the coating (quarter-wave coating), where n_a and n_s are the refractive indices of the air ($n_a = 1.00$) and the substrate, respectively. (ii) $d = \lambda/4n_c$, d is the thickness of the coating, λ is the wavelength of incident light, and n_c is the refractive index of coating. Nanoporous films with a low refractive index (approximately 1.22) and a quarter-wave coating are often used as AR films and coatings on glass or transparent plastic substrates with a refractive index of approximately 1.5 [8, 11]. Antifogging (AF) and AR coatings can maintain good visibility at all times, even in extreme climates with high temperature and humidity. Therefore, their preparation is becoming a subject of intense

https://doi.org/10.1557/jmr.2019.309 Published online by Cambridge University Press

© Materials Research Society 2019

study for scientists and engineers [9, 12]. Various methods, such as layer-by-layer (LbL) assembly, dip-coating, spin-coating, spray-coating, and chemical modification, are often adopted in building antireflection [8, 9, 12, 13], in self-cleaning (SC) [11, 14, 15, 16], and in the preparation for AF [5, 16, 17, 18, 19].

Electrostatic LbL self-assembly, which was first reported by Iler in 1966 [20], is a simple, effective, and inexpensive method to fabricate various kinds of coatings [21, 22, 23]. To greatly improve the efficiency of an assembly process, Merrill and Sun [24] first adopted the spin-spray layer-by-layer (SSLbL) assembly method. In this article, we have employed a modified SSLbL assembly method to rapidly produce thin coatings. During a spin state, the coatings were blown dry with hot air to speed up the LbL assembly process. We called this spray-spin-blow layer-by-layer (SSBLbL) assembly. While both processes are simple, rapid, and highly efficient methods to produce ultrathin coating [25, 26], they also reduce the consumption of materials [24, 27]. ZrO_2 and SiO_2 nanoparticles (NPs) were designed, synthesized, and utilized as building materials. They are of great interest due to their wide applications in almost all fields of industry. They are known as chemically stable, nontoxic, and eco-friendly NPs, and in addition, they are inexpensive and abundant in the nature. Thus, they are used in practically all fields of science and engineering and in everyday life as well.

In this work, we attempt to demonstrate that stable AF, AR, and SC coatings can be easily and quickly fabricated onto glass substrates using a spray-spin-blow LbL assembly method. This consisted of alternatingly applying three bilayers of positively charged ZrO_2 NPs and negatively charged SiO_2 NPs. The layers were firmly and quickly bound together via electrostatic interactions. The SSBLbL method is powerful yet simple, practical, and easy-to-use, and enables a high-throughput. The major advantage of the method is a dramatically reduced processing time needed for the multilayer formation, and the consumption of materials [24, 27]. The high-temperature calcination can remove organics and impurities of the surface, promote the formation of stable siloxane bridges along with enhanced mechanical stability and adhesion to the substrates, and introduce three-dimensional (3D) nanoporous networks in the coating along with hydrophilicity improvement [4]. These are essential features required for AF, AR, and SC coatings. As investigated in previous studies, such multifunctional coatings fabricated by SSBLbL electrostatic assembly of alternating positively charged ZrO_2 NPs and negatively charged SiO_2 NPs, exhibiting excellent superhydrophilic, AF, AR, and SC properties, have not yet been reported. Preparation of these multifunctional coatings should become a focus of research due to its potential and promising applications in various fields.

Results and discussion

NP morphology and structure, and zeta potential measurements

The microstructure and morphology of SiO_2 and ZrO_2 NPs were characterized by a transmission electron microscope (TEM); the particle size and morphology are of great importance for the performance of the coatings. As shown in Figs. 1(a) and 1(b), the SiO_2 particles with uniform shape are monodisperse spheres of average diameter of approximately 45 nm. For comparison, we also used a Zetasizer Nano-ZS (Malvern instruments, Malvern, U.K.) to measure the same sample. The size of the SiO_2 NPs [44.6 nm; see Fig. 2], polydispersity index (PDI) = 0.047, and zeta potential

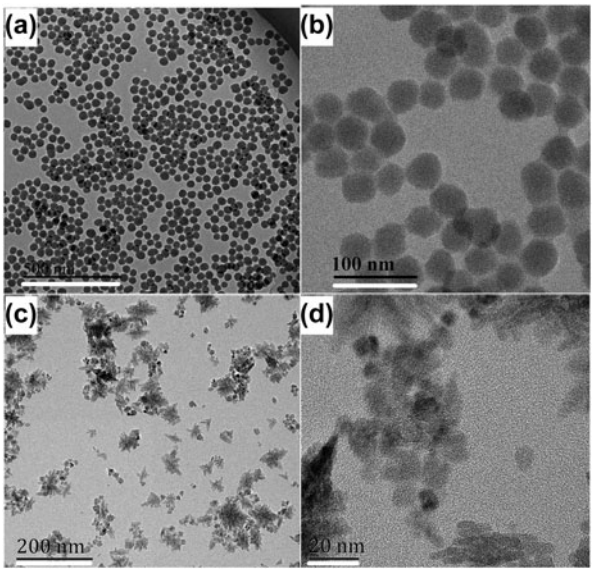


Figure 1: TEM images of NPs of (a) SiO_2 and (c) ZrO_2, (b) and (d) are magnified views of (a) and (c), respectively. The scale bar in (a), (b), (c), and (d) is 500, 100, 200, and 20 nm, respectively.

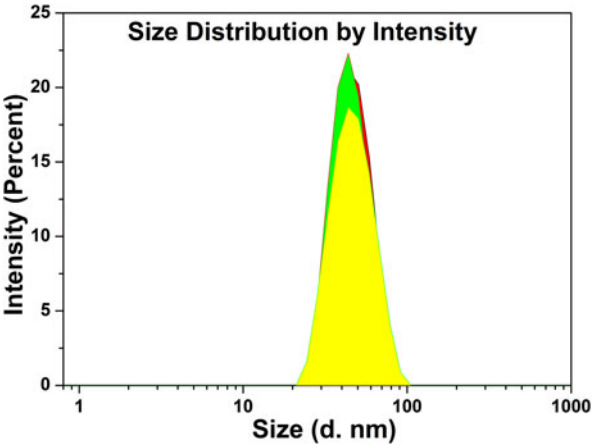


Figure 2: Particle size graph of SiO_2 NPs (mean value: 44.6 nm, PDI, 0.047).

https://doi.org/10.1557/jmr.2019.309 Published online by Cambridge University Press

© Materials Research Society 2019

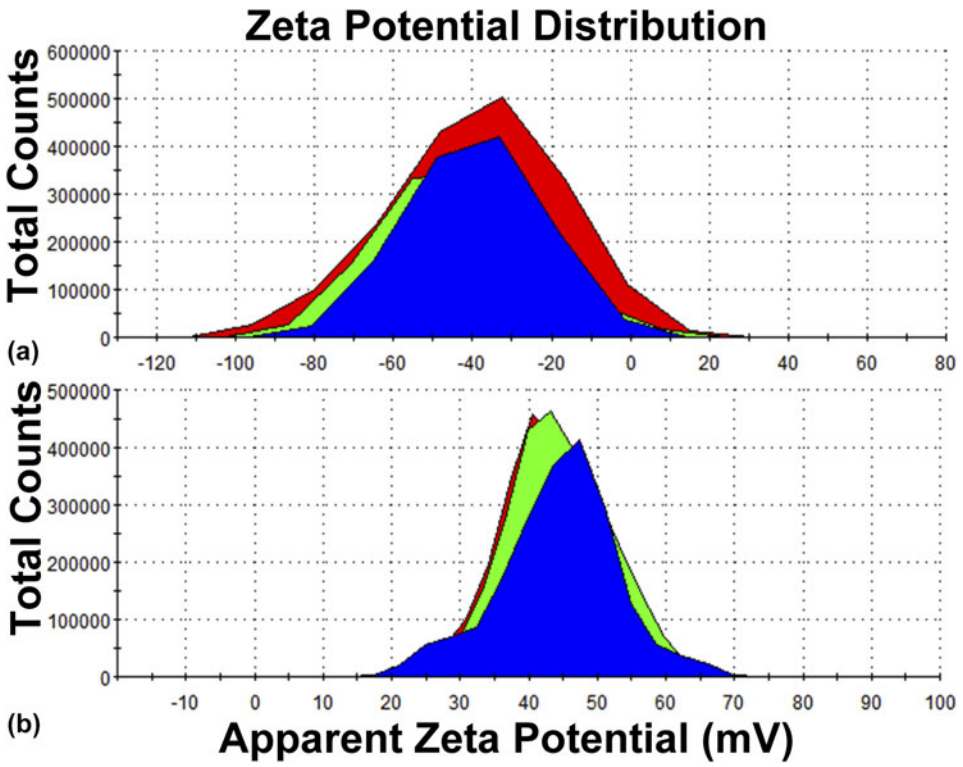


Figure 3: Zeta potential graphs of (a) SiO_2 NPs (mean value: −40.9 mV) and (b) ZrO_2 NPs (mean value: +43.3 mV).

[−40.9 mV; Fig. 3(a)] were obtained and these data were measured in triplicate for accuracy. It was noted that the data from the Zetasizer Nano-ZS instrument were in agreement with the TEM results. The morphologies of the ZrO_2 NPs characterized by TEM are shown in Figs. 1(c) and 1(d), from which we can see clearly that ZrO_2 with good dispersion in nanoscale particles are also dispersed well. The shape of ZrO_2 NPs in granular form is not as regular as that of spherical SiO_2 NPs. The crystalline phase structures of SiO_2 and ZrO_2 NPs were determined by X-ray powder diffraction (XRD), as shown in Fig. 4. The results demonstrated that silica NPs had a typical characteristic amorphous peak [approximately 22°; see Fig. 4(a)], and zirconia was a structure of the typical monoclinic phase, as shown in Fig. 4(b). The zeta potentials of SiO_2 and ZrO_2 NPs were measured at 25 °C with a Zetasizer Nano-ZS instrument. It is an essential parameter for the characterization of the stability of an NP solution. A minimum of ±30 mV zeta potential value is required for indication of stable nanosol [28]. The SiO_2 and ZrO_2 had ζ-potential of −40.9 mV and +43.3 mV, respectively [see Figs. 3(a) and 3(b)].

ZrO_2/SiO_2 multilayer assembly and calcination of the coatings

Multifunctional AF coatings can be readily fabricated from SSBLbL assembled films of positively charged ZrO_2 and negatively charged SiO_2 NPs. They are bound firmly together via electrostatic interactions. The concentration of both ZrO_2 and SiO_2 NP solutions was 0.8 mg/mL, with reference to previous studies [24, 25, 26]. The positively charged ZrO_2 (+43.3 mV) and negatively charged SiO_2 solutions (−40.9 mV) were alternately sprayed on the spinning substrate, followed by blowing dry hot air after each step (see the schematic diagram in Fig. 5). Finally, the as-prepared coatings were calcined (heating rate: 2 °C/min) in a muffle furnace for 2.5 h. For long-term applications, they need to have excellent adhesion to the underlying substrates and good mechanical durability for daily use. Hence, high-temperature calcination is used for this purpose. The high-temperature treatment can fuse the NPs with one another and with glass substrates via the formation of

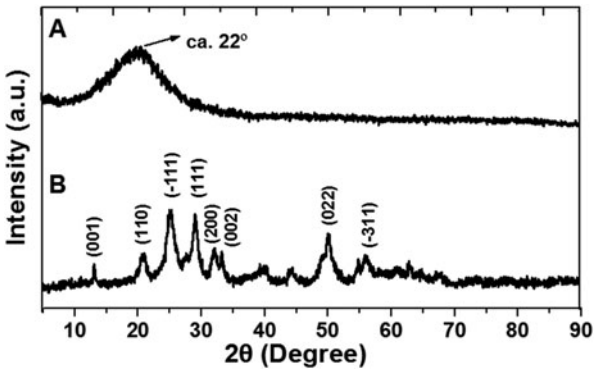


Figure 4: XRD patterns of (a) SiO_2 and (b) ZrO_2 NPs calcined at 520 °C.

https://doi.org/10.1557/jmr.2019.309 Published online by Cambridge University Press

© Materials Research Society 2019

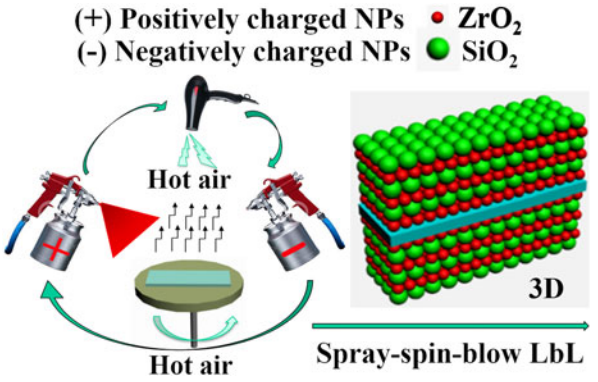


Figure 5: Schematic of a spray-spin-blow LbL assembly process to create multifunctional AF coatings on a substrate.

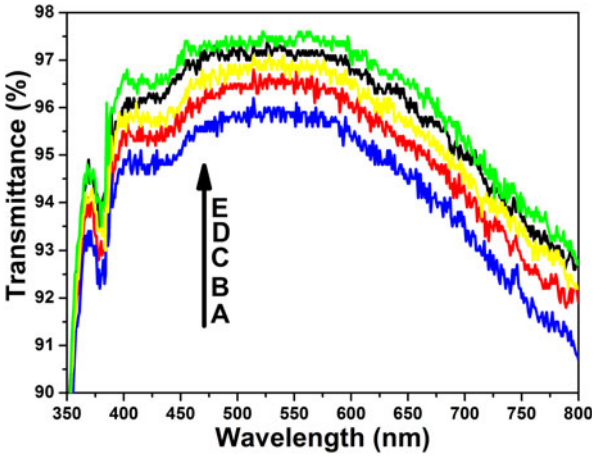


Figure 6: UV-Vis transmission spectra of ZrO_2/SiO_2 coatings on glass substrates with different calcination temperatures: (a) 400, (b) 440, (c) 480, (d) 520, and (e) 560 °C.

stable siloxane bridges. After this treatment, the mechanical stability of the resultant coatings can be increased tremendously along with hydrophilicity improvement. In order to create an ideal AR coating with permanent AF properties, we investigated the effects of the number of deposited bilayers and different calcination temperatures. The preferred number of bilayers in an assembly was three, which will be described below in detail. To assess the effects of calcination temperatures on the transmittance and superhydrophilicity of the coatings, we prepared a series of coatings with three bilayers, which were calcined in a muffle furnace at 400, 440, 480, 520, and 560 °C for 2.5 h. As seen in Fig. 6, compared with the spectra (380–780 nm) of a bare glass (90.6% in transmittance), the average transmittance values of the coatings at different calcination temperatures were approximately 95.4%, 95.9%, 96.3%, 96.7%, and 96.8%, respectively. No apparent difference in transmittance (less than 1.4%) was observed when the temperature was increased from 400 to 560 °C. In the water contact angle (WCA) test, all the coatings formed at different calcination temperatures exhibited excellent superhydrophilicity (close to 0°, <0.04 s). This was because the high-temperature calcination (more than 400 °C) could burn out organics and impurities from the substrate surface, and retain hydrophilic inorganic materials and a 3D nanoporous network texture on the surface. Owing to the temperature of more than approximately 560 °C, glass can undergo thermal deformation. For rapid and high-efficiency preparation, the temperature of 520 °C was chosen as an optimum temperature in all the following experiments. The ZrO_2/SiO_2 coatings were fabricated with the ZrO_2 coating as the first layer; after three bilayer stacks on each side, the ZrO_2/SiO_2 coatings were then calcined at 520 °C for 2.5 h. For comparison, the SiO_2/ZrO_2 coatings (the SiO_2 coating was the first layer) were also prepared under the same conditions. After various performance tests, it was found that although the SiO_2/ZrO_2 coatings had excellent superhydrophilic behavior, the ZrO_2/SiO_2 coatings had better properties than the former with regard to AF, transmission, and mechanical stability. This was because of the small-size ZrO_2 NPs on the bottom layer and in the inner layers, which led to more ZrO_2 NPs in ZrO_2/SiO_2 coatings than SiO_2/ZrO_2 coatings. The ZrO_2 NPs, which were smaller in size and carried a positive electrical charge, could greatly reduce light scattering and could more easily produce more nanoporosity and nano-roughness [10]; likewise, they could more easily absorb water with negative charge for electrostatic attractions.

Optical characterization and AR properties

Optical clarity is of great importance for optical and display devices, and it is highly desired in practical applications. Optical coatings can reduce reflection and enhance transmission, and thus have attracted a great deal of interest in industrial and academic fields [8, 12]. The optical performances of the coatings are evaluated by transmittance measurements in the visible region. A good antireflection coating should show an overall high transmittance over the entire visible region, and not at a specific point or within a certain wavelength range. This may impart color to the glass due to visible absorption. The coated nanoporous structure (low refractive index) and coating thickness are believed to affect the transmittance of coatings, through packing of different sizes of ZrO_2 and SiO_2 NPs; nanopores (n_a = 1.00) are introduced to lower the refractive index of the coating. When the refractive index is 1.22, the wavelength of maximum suppression is determined by the quarter-wave optical thickness of the coating. The quarter-wave coating, in turn, can be tuned over the entire visible region by simply controlling the number of bilayer stacks. In order to better understand the relationship between transmittance and the number of bilayer stacks, we prepared a series of coatings that contained 1, 2, 3, and 4 bilayers of ZrO_2/SiO_2 coatings calcined at 520 °C. Fig. 7 shows the

https://doi.org/10.1557/jmr.2019.309 Published online by Cambridge University Press

© Materials Research Society 2019

transmission spectra of ZrO_2/SiO_2 multilayer coatings with different bilayer stacks on a glass substrate in the spectral range between 350 and 800 nm, and a bare glass is used for comparison. With the increase in the number of stacks, the average transmittance values in the visible region (380–780 nm) were increased to approximately 93.3%, 95.2%, 96.7%, and 96.9%, respectively. The transmittance values increased significantly compared with that of the bare glass (90.6%). This may be attributed to the coating thickness and the surface nanoporous structure (low refractive index). When the transmittance increases to 96.7% (three stacks), the coating thickness is near the quarter-wave coating [approximately 140 nm, see Fig. 8(d)], and therefore, there is little increase in transmittance (0.2%) for four stacks. For rapid and high-efficiency preparation, the three stacks were chosen as an optimum condition to study the coating properties.

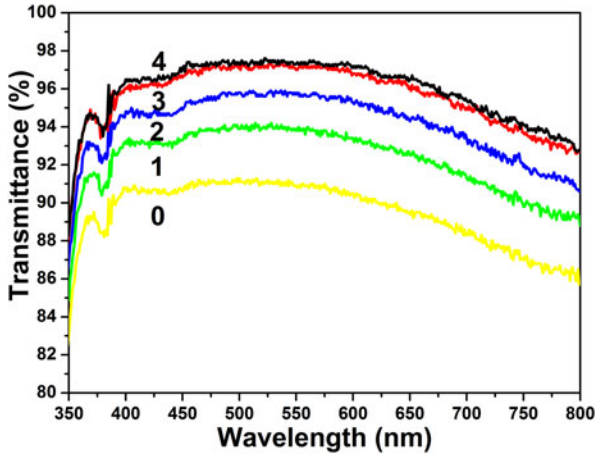


Figure 7: UV-Vis transmission spectra of ZrO_2/SiO_2 coatings on glass substrates with 1–4 bilayer stacks calcined at 520 °C, and a bare glass (0) provided for comparison.

Morphology and structure of multifunctional AF coatings

Surface texture (surface roughness and void space) is believed to affect both the transmittance and wetting property of the coating. Using a SSBLbL assembly of different sizes of ZrO_2 and SiO_2 NPs, a 3D nanoporous network texture is introduced to the surface of the coating. SEM images in Fig. 8 show the surface morphologies and structures of ZrO_2/SiO_2 coatings. Two kinds of NPs of different sizes can be seen clearly, and their mutual assembly can increase the surface roughness and nanoporosity. Top-view SEM images [Figs. 8(a) and 8(b)] show that the glass substrate was homogeneously covered by ZrO_2 and SiO_2 NPs; most obviously, the SiO_2 NPs, which are of bigger size, are spherical particles of uniform size. The magnified SEM image of the coating [Fig. 8(c)] reveals that the dense pores with sizes between 20 and 50 nm are clearly observed in the coating. The size of the SiO_2 NPs is approximately 55 nm in the SEM images [Figs. 8(a)–8(c)], but this is

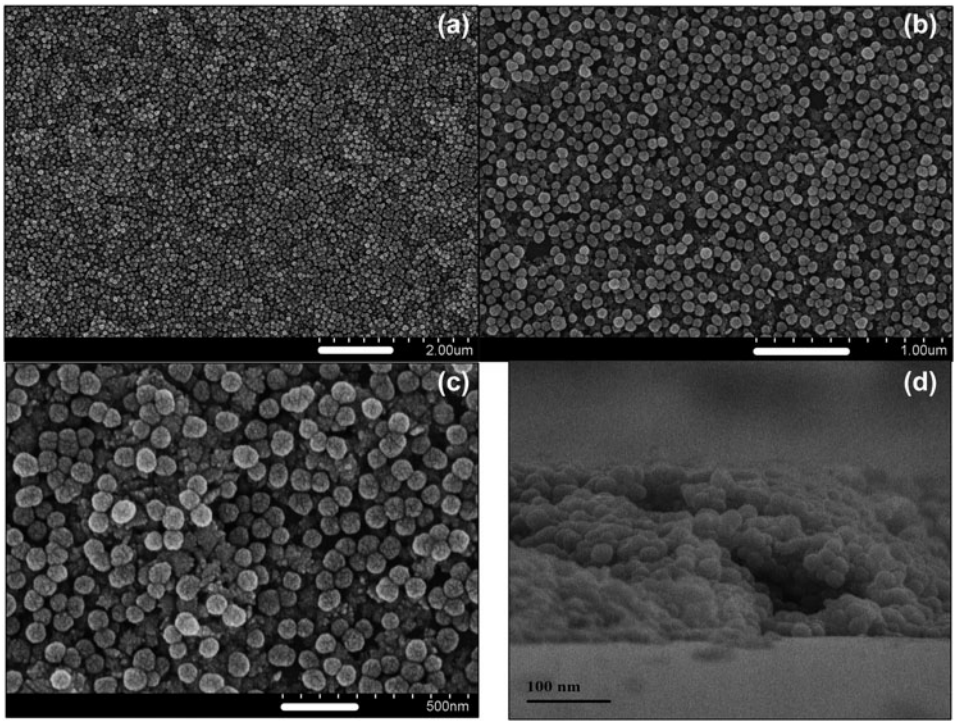


Figure 8: SEM images of spray-spin-blow LbL assembled (a) ZrO_2/SiO_2 coatings. (b) and (c) are the magnified images of the coatings. (d) Cross-sectional SEM image of the multifunctional AF coatings. The scale bar in (a), (b), (c), and (d) is 1000, 500, 200, and 100 nm, respectively.

https://doi.org/10.1557/jmr.2019.309 Published online by Cambridge University Press

© Materials Research Society 2019

not the real particle size; the true size is approximately 45 nm because the sample surface was covered by gold NPs. In order to reduce charging effects that are caused by high-power electron beams during examinations, the sample was gold-plated using a sputter coater, and the thickness of the gold coating was approximately 10 nm. The three images [Figs. 8(a)–8(c)] were captured from different positions, and the size of the SiO_2 NPs is in agreement with the data from the TEM (approximately 45 nm) and Zetasizer Nano-ZS instrument (44.6 nm). From the SEM images, we can see that the ZrO_2/SiO_2 coatings have a high nano-roughness surface, which has a 3D interconnected nanoporous network structure. It is noted that the coated surface with raspberry-like, mulberry-like, or cauliflower-like particles is not the real surface topography; most of the particles on the surface are Au nanocluster particles. From a cross-sectional SEM image [Fig. 8(d)], it could be seen that the spherical SiO_2 NPs were connected to one another and densely packed on the surface. The average thickness of the coatings was approximately 140 nm. It should be noted that the ZrO_2 NPs with positive electrical charge in the coating are more attracted to water with negative charge due to electrostatic attractions. Overall, the coating with a nano-roughness surface and an appropriate thickness can exhibit exciting superhydrophilic/AF and antireflection properties.

AF/superhydrophilic performances

The superhydrophilicity of solid surfaces is currently receiving a lot of attention in material science because of its scientific significance and numerous potential applications. According to the early theoretical work by Wenzel [29] and Cassie–Baxter [30], and more recent studies by Quéré and coworkers [31, 32], the textured surfaces and void fraction can significantly enhance the wettability of surfaces with water. This may result in enhanced AF properties. As is well known to all scholars working in the field, the superhydrophilic coatings/superhydrophilicity can significantly inhibit fogging by preventing light-scattering water droplets from forming on a substrate surface. In this work, the coating surface was instantaneously and thoroughly wetted by water and thus covered with a thin sheet-like water membrane. The transparent water membrane eventually disappeared either by sliding down under the action of gravity or by evaporation. Thus, the coating surface could effectively maintain optical transparency. The AF/superhydrophilic performances were investigated using a WCA test, a boiling test, and a low-temperature AF test.

WCAs were carried out at room temperature using a Krüss DSA 30 system, and the average WCA value was obtained by measuring more than five different positions on each sample. The spreading process of the water droplet was recorded by a CCD camera with a frame rate of 25 frames/s. A water droplet of 3 μL was dropped carefully onto the sample; once the water droplet contacted the sample surface, the machine began to take photographs at 25 frames/s (time interval between frames 40 ms). As soon as the first water droplet contacted the ZrO_2/SiO_2 coating, it spread flat instantaneously to form a thin sheet-like water membrane in less than 0.04 s [Fig. 9(a)]. The water droplet dripping moment [marked "#" in Fig. 9(a)] was captured by the CCD camera. This confirmed that the coating was superhydrophilic. A video of the AF/superhydrophilic behavior is presented in Supplementary material (Movie S1).

In the boiling test (constant 100 °C), the experiment was carried out using more than five parallel samples to ensure accuracy, and results were obtained. As seen in Fig. 9(b), the coated slide (red clip) always remained visible. The words at the bottom of the beaker remained visible. In sharp contrast, nothing can be seen through the bare glass slide (blue clip). The experiment was maintained constant at 100 °C for 8 h. The results confirmed that ZrO_2/SiO_2 coatings had excellent AF performance, much more than expected. This was because the nearly instantaneous, sheet-like wetting by water prevented light-scattering water droplets from forming on the substrate surface. It is noted that the ZrO_2 NPs carry positive electrical charges, and water carries negative charges. The ZrO_2 NPs with

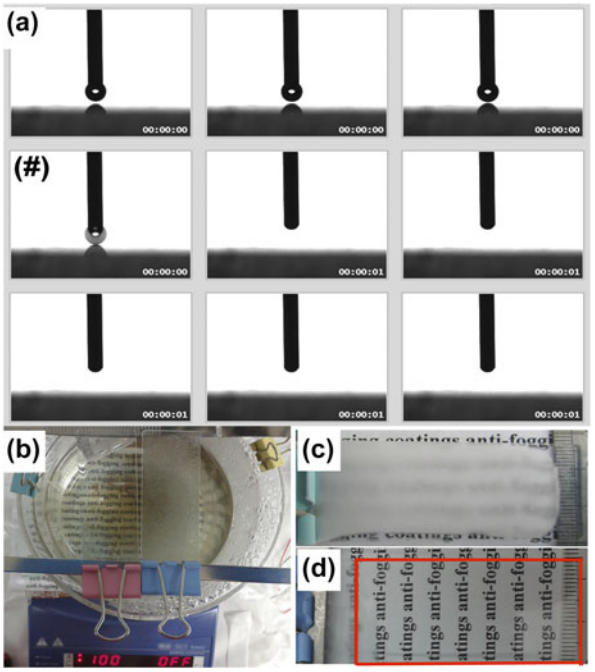


Figure 9: (a) Still images captured from video recordings for a water droplet (3 μL) spreading on a substrate covered with multifunctional AF coatings. (b) Photo image of the boiling test. Comparison of the AF behavior of ZrO_2/SiO_2 coatings (red clip) with a bare glass slide (blue clip). Photo images of a bare glass (c) and the substrate coated with ZrO_2/SiO_2 coatings (d) after being stored at −15 °C for 3 h in a freezer.

https://doi.org/10.1557/jmr.2019.309 Published online by Cambridge University Press

© Materials Research Society 2019

positive electrical charge on the bottom are more attracted to the negatively charged water due to electrostatic attractions [3]. This can contribute to improving the hydrophilic effect.

In the low temperature AF test, the samples (more than five parallel samples) were stored in a freezer at −15 °C for 3 h, and then all samples were simultaneously exposed to humid air (approximately 20 °C and 65% relative humidity (RH)). As revealed in Figs. 9(c) and 9(d), the bare glass slide [Fig. 9(c)] covered with heavy frost and the words below are completely invisible due to strong light scattering. In sharp contrast, the substrates coated with ZrO_2/SiO_2 [Fig. 9(d)] coatings can remain highly transparent and the words below can be seen clearly (red wireframe) because the superhydrophilic surface can prevent the formation of light-scattering tiny ice droplets which are capable of scattering light randomly on a surface. The results of these tests confirmed that the ZrO_2/SiO_2 coatings with rough surface and nanovoids exhibited exciting superhydrophilic and AF properties.

SC/easy-to-clean performances and mechanical stability

AF and AR coatings, as well as SC/easy-to-clean properties may be of advantage in certain applications. The SC/easy-to-clean effect is obtained when a substrate surface is superhydrophilic (water dissolves contaminants and washes them away more easily) or superhydrophobic (water forms balls and carries away contaminants). It is always associated with long-term stability of the coating, which is an important parameter for evaluating the coating performance. The durability of the SSBLbL electrostatically assembled ZrO_2/SiO_2 coatings was investigated by an outdoor test over a year, as shown in Figs. 10(a) and 10(b). The vertically placed samples (with dimensions of approximately 12 × 6 cm) were kept in an actual outdoor environment and suffered from wind and weather during the test. The coated and uncoated glass surfaces were captured by a digital camera (IXUS130; Canon, Tokyo, Japan) in Fig. 10(e). However, it was very difficult to take photographs for contaminants on the glass surface which was transparent. We used a light brown rough wall as a background, and positioned a camera at a certain angle to capture the contaminants on the glass surface. As seen in Fig. 10(e), the uncoated glass (left) has much contaminants on the surface, yet there were few contaminants on the coated glass (right). This is because the superhydrophilic surface of the ZrO_2/SiO_2 coating makes the water spread over the surface completely and instantaneously. At the same time, the coated surface absorbs the water molecules more easily. This combination makes it easier to dissolve the contaminants and wash them away. Figures 10(a) and 10(b) show the transmittance values of the outdoor test: the solid line [Fig. 10(a)] and dotted line [Fig. 10(b)] show the transmittance of the ZrO_2/SiO_2 sample before and after the outdoor test (investigated for more than a year), respectively. No apparent decrease (less than 1.8%) in transmittance was seen over a year. In the WCA test, the water droplet took a little longer time (~0.3 s) to completely spread on the coatings left in outdoor service for more than a year. It shows that the multifunctional AF coatings have excellent stability after long-term service.

The mechanical stability of the SSBLbL electrostatically assembled ZrO_2/SiO_2 coating was investigated by a pencil hardness test and a sandpaper abrasion test. In the pencil hardness test, the results confirmed that the ZrO_2/SiO_2 samples achieved more than 4H pencil hardness (ASTM D3363-05). In the sandpaper abrasion test, the sample was moved back and forth (1 abrasion cycle) under a 100-g load for a constant 10 cm on a sandpaper (grit No. 320). Hundred abrasion cycles were applied to each side. The abrasion resistance was evaluated by comparing the transmittance values before and after the tests, as shown in Figs. 10(c) and 10(d). The solid line [Fig. 10(c)] and dotted line [Fig. 10(d)] show the transmittance of the ZrO_2/SiO_2 sample before and after the abrasion test, respectively. There is no observable decrease in transmittance in the visible region and the thickness of the coatings still remains unchanged (approximately 140 nm). We also investigated the AF behavior: the ZrO_2/SiO_2 samples after the abrasion test still had a good AF effect (approximately 0°, <0.04 s). Hence, we have demonstrated a simple coating which exhibits excellent SC/easy-to-clean and AF properties due to the superhydrophilicity of the coating.

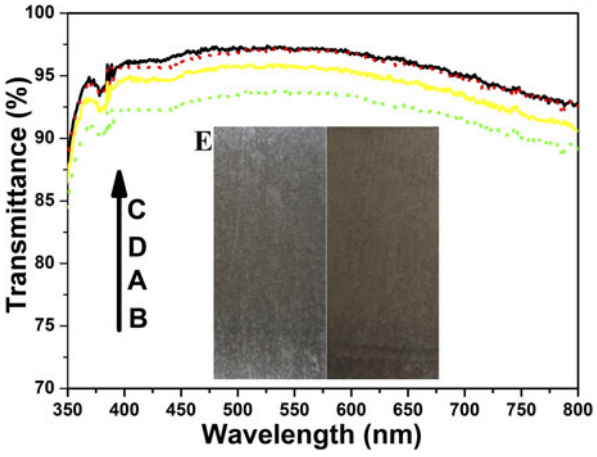


Figure 10: UV-Vis transmission spectra of the ZrO_2/SiO_2 sample before (a, solid line) and after (b, dot line) an outdoor test over a year. Comparison of the transmission spectra of the ZrO_2/SiO_2 sample before (c, solid line) and after (d, dotted line) the abrasion test. (e) Comparison of the contaminants on the glass surface of the ZrO_2/SiO_2-coated glass (right) and an uncoated glass (left) in an outdoor test over a year.

https://doi.org/10.1557/jmr.2019.309 Published online by Cambridge University Press

© Materials Research Society 2019

Conclusions

In this work, a novel, rapid, and high-efficiency spray-spin-blow LbL assembly technique has been developed for fabricating multifunctional AF coatings/films on glass substrates by three bilayer stacks of alternating positively charged ZrO_2 NPs and negatively charged SiO_2 NPs. The oppositely charged NPs were bound firmly together via electrostatic interactions. The high-temperature calcination (520 °C) removed organics and impurities from the surface, endowed the coating with enhanced mechanical robustness, and introduced 3D nanoporous networks in the resultant coating along with hydrophilicity improvement. The SSBLbL assembly technique, combined with very tight process control, presented a simple, efficient, and low-cost nanomanufacturing capability to produce coatings/films. The resultant coatings exhibited excellent AF and SC properties due to the superhydrophilicity of the coating, showed excellent AR properties due to a suitable coating thickness and the low refractive index coating formed from the nanoporous morphology (n_{air} = 1.00), and exhibited excellent superhydrophilic properties due to a 3D nanoporous network texture. Meanwhile, we have confirmed that the AF, superhydrophilic, AR, and SC properties, as well as high mechanical stability can be integrated into the same coating consisting of ZrO_2 and SiO_2 NPs. The simplicity of the fabrication process, easy availability of the nanomaterials, and excellent adhesion to substrates for the coating preparation might make the low-cost, nontoxic, and eco-friendly multifunctional coatings potentially useful in optical and display devices.

Experimental section

Materials

All chemicals in this study were used as purchased; tetraethyl orthosilicate (TEOS; 98+%), aqueous ammonia (NH_3, 28%), concentrated sulfuric acid (95–98 wt%), hydrogen peroxide (30%), zirconyl oxychloride ($ZrOCl_2{\cdot}8H_2O$, 99%), and anhydrous ethanol (99.80%) were all obtained from Sinopharm Chemical Reagent Co., Ltd. (Shanghai, China). Ultrapure water was obtained from a three-stage Millipore Mill-Q Plus 185 purification system (Academic, resistivity higher than 18.2 MΩ·cm).

Preparation of monodisperse SiO_2 NPs

SiO_2 NPs of approximately 45 nm in size were prepared as follows [3, 33]. 100 mL anhydrous ethanol and 3.2 mL aqueous ammonia were mixed with stirring in a round-bottomed flask at room temperature in a water bath, and then 2.1 mL of TEOS was added dropwise to the solution under stirring at 1500 rpm for 15 min. Afterward, the temperature was increased to 30 °C and kept at this temperature under magnetic stirring at 500 rpm for 48 h. Finally, the ethanol suspension of silica NPs of approximately 45 nm size was obtained. The as-prepared SiO_2 sol was diluted in ethanol and ultra-sonicated before use. The final concentration of silica was 0.8 mg/mL, and it had a −40.9 mV zeta potential and 44.6 nm size [PDI = 0.047] as measured by a Malvern Zetasizer Nano-ZS instrument.

Preparation of ZrO_2 NPs

With reference to previous studies [3, 34, 35], ZrO_2 NPs were synthesized using a modified hydrothermal method as follows: 85 mL $ZrOCl_2{\cdot}8H_2O$ (0.1 M) and 70 mL anhydrous ethanol were mixed in a beaker by magnetic stirring for 15 min at room temperature. Then the solution was transferred into a Teflon-lined stainless-steel autoclave (200 mL capacity) and heated at 195 °C for 16 h. After the autoclave was cooled down to room temperature naturally, the product was purified by centrifugation and redispersed in ethanol via an ultrasonication-assisted process. The ZrO_2 was diluted in ethanol to a final concentration of 0.8 mg/mL. Afterward, the zeta potential was measured using a Zetasizer Nano-ZS instrument, and it had a +43.3-mV zeta potential value.

Fabrication of multifunctional AF coatings

Glass microscope slides (SAIL BRAND Cat. No. 7101) with dimensions of approximately 25.4 × 76.2 × 1 mm were immersed in a slightly boiled piranha solution (70/30 v/v of 98 wt% H_2SO_4/30 wt% H_2O_2; caution: piranha solution reacts violently with organic compounds and should not be stored in closed containers) for 6 h, then rinsed with ultrapure water and ethanol, and then blown dry under nitrogen. The cleaned glass slides were obtained and used as substrates in the following experiments. Multifunctional coatings were fabricated using a SSBLbL assembly process, and this process is driven by electrostatic interactions between the positively charged ZrO_2 NPs (+43.3 mV) and negatively charged SiO_2 NPs (−40.9 mV). As seen in Fig. 5, a glass substrate was held on a vacuum chuck and spun at 1500 rpm throughout all steps of the spray-spin-blow process to ensure even coverage. The spray nozzle diameter was 0.3 mm, and the distance between the substrate and the nozzle was fixed to 15 cm; the positively charged ZrO_2 nanosol (+43.3 mV) and negatively charged SiO_2 nanosol (−40.9 mV) were alternately sprayed on the substrate. Between each layer deposition, the film was blown dry with hot air for 10 s to ensure complete drying. The spray time was 1.5 s for both ZrO_2 nanosol and SiO_2 nanosol with a spray pressure of 10 psi (69 kPa). A typical bilayer was assembled as follows. The substrate was spun constantly at 1500 rpm throughout all four steps to ensure the formation of an evenly thin film. The positively charged ZrO_2 nanosol was sprayed for 1.5 s to render the substrate surface to be charged.

https://doi.org/10.1557/jmr.2019.309 Published online by Cambridge University Press

© Materials Research Society 2019

Next, the film was blown dry with hot air for 10 s while spinning. Then, the negatively charged SiO_2 nanosol (−40.9 mV) was also sprayed for 1.5 s, followed by drying for another 10 s. In this way, one positively charged ZrO_2 inner layer and one negatively charged SiO_2 outer layer were fabricated due to electrostatic interactions. If desired, a washing step can be incorporated before the drying step. This process completed one cycle of SSBLbL assembly to form a single bilayer of ZrO_2 NPs and SiO_2 NPs. The same process was then repeated until the desired number of bilayers was achieved. The other side of the glass substrate was treated in the same way as above. Finally, the as-prepared coatings were calcined (heating rate: 2 °C/min) in a muffle furnace for 2.5 h to remove organics and improve their adhesion to the substrate. They were then subsequently cooled down to room temperature with a cooling rate of 3 °C/min.

Characterization methods for multifunctional AF coatings

The morphology and size of SiO_2 and ZrO_2 NPs were observed using a transmission electron microscope (TEM; JEM-2100, JEOL, Tokyo, Japan) with an acceleration voltage of 200 kV equipped with a Gatan CCD camera. Surface morphology and cross section of the coatings were investigated using a field-emission scanning electron microscope (FE-SEM; Hitachi S-4800, Tokyo, Japan) operated at an acceleration voltage of 5 kV. Prior to imaging, the samples were sputtered with gold to reduce charging effects during examinations. The zeta potential and particle size were measured in triplicate using a Zetasizer Nano-ZS (Malvern instruments, Malvern, U.K.) at a temperature of 25 °C. The X-ray powder diffraction (XRD) data were collected at room temperature using a D/Max-2550 PC diffractometer (Rigaku, Japan) equipped with an X-ray tube (Cu K_α radiation: $\lambda = 1.5406$ Å; 40 kV, 200 mA) to identify the crystalline phases of the samples. Transmission spectra in the range between 350 and 800 nm were performed using a U-3310 UV-Vis spectrophotometer (Hitachi Co., Ltd., Japan) at a RH of approximately 30%. WCAs of surfaces were measured at an ambient temperature using a Krüss DSA 30 drop shape analysis system (Krüss GmbH, Hamburg, Germany), and a water droplet (>18.2 MΩ cm) of 3 μL was dropped carefully onto the sample surface and also used as the indicator to characterize the wetting property of the coating. The spreading process of the water droplet was recorded by a CCD camera at a capture speed of 25 frames/s. AF properties were evaluated by two methods. One was a boiling test [3], in which the samples were placed on the top of a beaker containing boiling water (80% full), and vapor condensed on the coating surface was observed and photographed. The other was a low temperature AF test, in which the samples were stored in a freezer at −15 °C for 3 h and then exposed to humid air (at 20 ± 3 °C and 65 ± 5% RH) simultaneously to observe whether fog was formed on the coating. An electric furnace (HMX1100-20, Shanghai Haoyue Electric Technology Co., Ltd., Shanghai, China) was used to calcinate the coatings. A digital camera (IXUS130; Canon, Tokyo, Japan) was used to capture the images.

Acknowledgments

This work was supported partially by the Key Research and Development Plan Project of Anhui Province (Grant No. 1804a09020077).

Supplementary material

To view supplementary material for this article, please visit https://doi.org/10.1557/jmr.2019.309.

References

1. **N. Nuraje, R. Asmatulu, R.E. Cohen, and M.F. Rubner**: Durable antifog films from layer-by-layer molecularly blended hydrophilic polysaccharides. *Langmuir* **27**, 782 (2011).
2. **C-C. Chang, F-H. Huang, H-H. Chang, T-M. Don, C-C. Chen, and L-P. Cheng**: Preparation of water-resistant antifog hard coatings on plastic substrate. *Langmuir* **28**, 17193 (2012).
3. **F. Yang, P. Wang, X. Yang, and Z. Cai**: Antifogging and anti-frosting coatings by dip-layer-by-layer self-assembly of just triple-layer oppositely charged nanoparticles. *Thin solid films* **634**, 85 (2017).
4. **F.Ç. Cebeci, Z. Wu, L. Zhai, R.E. Cohen, and M.F. Rubner**: Nanoporosity-driven superhydrophilicity: A means to create multifunctional antifogging coatings. *Langmuir* **22**, 2856 (2006).
5. **L. Xu and J. He**: Antifogging and antireflection coatings fabricated by integrating solid and mesoporous silica nanoparticles without any post-treatments. *ACS Appl. Mater. Interfaces* **4**, 3293 (2012).
6. **A. Lafuma and D. Quere**: Superhydrophobic states. *Nat. Mater.* **2**, 457 (2003).
7. **X. Deng, L. Mammen, Y. Zhao, P. Lellig, K. Müllen, C. Li, H.J. Butt, and D. Vollmer**: Transparent, thermally stable and mechanically robust superhydrophobic surfaces made from porous silica capsules. *Adv. Mater.* **23**, 2962 (2011).
8. **P. Buskens, M. Burghoorn, M.C.D. Mourad, and Z. Vroon**: Antireflective coatings for glass and transparent polymers. *Langmuir* **32**, 6781 (2016).
9. **M. Mazur, D. Wojcieszak, D. Kaczmarek, J. Domaradzki, S. Song, D. Gibson, F. Placido, P. Mazur, M. Kalisz, and A. Poniedzialek**: Functional photocatalytically active and scratch resistant antireflective coating based on TiO_2 and SiO_2. *Appl. Surf. Sci.* **380**, 165 (2016).
10. **H.A. Macleod**: *Thin-Film Optical Filters* (CRC Press, London, New York, Washington, DC, 2001).

https://doi.org/10.1557/jmr.2019.309 Published online by Cambridge University Press

© Materials Research Society 2019

11. **X-T. Zhang, O. Sato, M. Taguchi, Y. Einaga, T. Murakami, and A. Fujishima**: Self-cleaning particle coating with antireflection properties. *Chem. Mater.* **17**, 696 (2005).
12. **L. Yao, J. He, Z. Geng, and T. Ren**: Fabrication of mechanically robust, self-cleaning and optically high-performance hybrid thin films by SiO_2 & TiO_2 double-shelled hollow nanospheres. *Nanoscale* **7**, 13125 (2015).
13. **J-H. You, B-I. Lee, J. Lee, H. Kim, and S-H. Byeon**: Superhydrophilic and antireflective $La(OH)_3/SiO_2$-nanorod/nanosphere films. *J. Colloid Interface Sci.* **354**, 373 (2011).
14. **Y. Jin, Q. Ke, P. Jiang, Y. Zhu, F. Cheng, and Y. Zhang**: Highly efficient oil/water separation and excellent self-cleaning surfaces based on 1-triacontanol-polymerized octadecylsiloxane coatings. *Appl. Surf. Sci.* **351**, 358 (2015).
15. **M. Liu, J. Li, Y. Hou, and Z. Guo**: Inorganic adhesives for robust superwetting surfaces. *ACS Nano* **11**, 1113 (2017).
16. **C. Thompson, R. Fleming, and M. Zou**: Transparent self-cleaning and antifogging silica nanoparticle films. *Sol. Energy Mater. Sol. Cells* **115**, 108 (2013).
17. **Q. Shang and Y. Zhou**: Fabrication of transparent superhydrophobic porous silica coating for self-cleaning and anti-fogging. *Ceram. Int.* **42**, 8706 (2016).
18. **W.J. Hsu, P.S. Huang, Y.C. Huang, S.W. Hu, H.K. Tsao, and D.Y. Kang**: Zeolite-based antifogging coating via direct wet deposition. *Langmuir* **35**, 2538 (2019).
19. **J.A. Howarter and J.P. Youngblood**: Self-cleaning and anti-fog surfaces via stimuli-responsive polymer brushes. *Adv. Mater.* **19**, 3838 (2007).
20. **R. Iler**: Multilayers of colloidal particles. *J. Colloid Interface Sci.* **21**, 569 (1966).
21. **J.J. Richardson, J. Cui, M. Björnmalm, J.A. Braunger, H. Ejima, and F. Caruso**: Innovation in layer-by-layer assembly. *Chem. Rev.* **116**, 14828 (2016).
22. **S. Zhang, C. Vlemincq, D. Ramirez Wong, D. Magnin, K. Glinel, S. Demoustier-Champagne, and A.M. Jonas**: Nanopapers of layer-by-layer nanotubes. *J. Mater. Chem. B* **4**, 7651 (2016).
23. **G. Decher**: Fuzzy nanoassemblies: Toward layered polymeric multicomposites. *Science* **277**, 1232 (1997).
24. **M.H. Merrill and C.T. Sun**: Fast, simple and efficient assembly of nanolayered materials and devices. *Nanotechnology* **20**, 075606 (2009).
25. **F.S. Gittleson, D. Hwang, W-H. Ryu, S.M. Hashmi, J. Hwang, T. Goh, and A.D. Taylor**: Ultrathin nanotube/nanowire electrodes by spin–spray layer-by-layer assembly: A concept for transparent energy storage. *ACS Nano* **9**, 10005 (2015).
26. **W. Ma, A. Soroush, T. Van Anh Luong, G. Brennan, M.S. Rahaman, B. Asadishad, and N. Tufenkji**: Spray- and spin-assisted layer-by-layer assembly of copper nanoparticles on thin-film composite reverse osmosis membrane for biofouling mitigation. *Water Res.* **99**, 188 (2016).
27. **M. Salomäki, T. Peltonen, and J. Kankare**: Multilayer films by spraying on spinning surface—Best of both worlds. *Thin solid films* **520**, 5550 (2012).
28. **C. Jacobs and R.H. Müller**: Production and characterization of a budesonide nanosuspension for pulmonary administration. *Pharm. Res.* **19**, 189 (2002).
29. **R.N. Wenzel**: Resistance of solid surfaces to wetting by water. *Ind. Eng. Chem.* **28**, 988 (1936).
30. **A.B.D. Cassie and S. Baxter**: Wettability of porous surfaces. *Trans. Faraday Soc.* **40**, 546 (1944).
31. **J. Bico, C. Marzolin, and D. Quéré**: Pearl drops. *Europhys. Lett.* **47**, 220 (1999).
32. **J. Bico, C. Tordeux, and D. Quéré**: Rough wetting. *Europhys. Lett.* **55**, 214 (2001).
33. **W. Stöber, A. Fink, and E. Bohn**: Controlled growth of monodisperse silica spheres in the micron size range. *J. Colloid Interface Sci.* **26**, 62 (1968).
34. **M.Z-C. Hu, M.T. Harris, and C.H. Byers**: Nucleation and growth for synthesis of nanometric zirconia particles by forced hydrolysis. *J. Colloid Interface Sci.* **198**, 87 (1998).
35. **L. Kumari, W. Li, J. Xu, R. Leblanc, D. Wang, Y. Li, H. Guo, and J. Zhang**: Controlled hydrothermal synthesis of zirconium oxide nanostructures and their optical properties. *Cryst. Growth Des.* **9**, 3874 (2009).

https://doi.org/10.1557/jmr.2019.309 Published online by Cambridge University Press

© Materials Research Society 2019